IEEE Access
Multidisciplinary ⋮ Rapid Review ⋮ Open Access Journal

Received 26 November 2022, accepted 21 December 2022, date of publication 26 December 2022,
date of current version 13 January 2023.

Digital Object Identifier 10.1109/ACCESS.2022.3232405

RESEARCH ARTICLE

Flood Forecasting Method Based on Improved VMD-FOS-QR-RBL

YANG LIU, LIHU WANG, SHUAIBING DU, LI ZHAO, AND XUEMEI LIU
School of Information Engineering, North China University of Water Resources and Electric Power, Zhengzhou 450046, China

Corresponding author: Lihu Wang (hellowanglihu@126.com)

This work was supported in part by the National Key Research and Development Project under Grant Strategic Research Projects in Key Areas 16, in part by the Water Conservancy Science and Technology Research Project in Henan Province Grant GG202042.

ABSTRACT To improve the accuracy, reliability and validity of flood prediction models, this study proposes a regularized broad learning (RBL) model based on an improved variational mode decomposition (VMD). Firstly, grey correlation analysis was used to improve the endpoint effect of the VMD and the particle swarm optimisation (PSO) algorithm was used to optimise the VMD parameters. Then, using orthogonal triangular decomposition (QR), redefining the hidden layer output of BL model and adding forgettable online sequence learning mechanism (FOS) to construct online sequence BL (FOS-QR-RBL), which can significantly improve the computational efficiency of BL model. Finally, a flood forecasting method based on improved VMD-FOS-QR-RBL was constructed by combining the FOS-QR-RBL with the improved VMD and applying it to regional flood forecasting. The experimental results show that the computational efficiency of FOS-QR-RBL is improved by 35% and 23.68% compared with RBL and QR-RBL, respectively. The mean absolute error (MAE) of the coupling model of VMD and FOS-QR-RBL is reduced by 80.30% and 84.10% respectively, and the nash efficiency coefficient (E_{ns}) is increased by 15.51% and 28.16% respectively, compared with that of the coupling model of FOS-QR-RBL with ensemble empirical mode decomposition (EEMD) and adaptive noise complete ensemble empirical mode decomposition (CEEMDAN). The results of the optimal operation based on VMD-FOS-OR-RBL show that the model can effectively reduce the economic losses caused by regional flooding.

INDEX TERMS Flood forecasting, broad learning, variational mode decomposition, orthogonal triangular decomposition.

I. INTRODUCTION

As a key aspect of water hazard control, accurate forecasting of river runoff is important. Under the influence of changing environment, the runoff formation process and evolution mechanism are complex and variable, and the basin steady-state assumption is no longer valid [1], [2]. Currently, it is important to explore disaster forecasting models suitable for different basins to achieve proactive and scientific flood control [3].

Flood forecasting studies mainly include mechanism-driven physical methods and statistical methods based on data science [4], [5]. Physical methods usually use physical parameters such as weather, runoff, and rainfall to construct mathematical models that can effectively capture hydrological characteristics and desired features [6]. For example, the Xinanjiang model is widely used for flood prediction in semi-humid areas because of its solid theoretical basis and ease of practice. However, the dynamic and non-smooth nature of hydrological evolution makes the model's multi-step accurate prediction accuracy low [7]. The distributed hydrological model effectively combines geographic information features and considers the spatial and temporal distribution heterogeneity of rainfall and subsurface conditions, which is currently one of the research hotspots of hydrological models. However, with the construction of a large number of small and medium-sized reservoirs, the scope of application of distributed hydrological models has been gradually restricted [8]. Compared with physical models, statistical models based on data science usually have the

The associate editor coordinating the review of this manuscript and approving it for publication was Varuna De Silva.

advantages of long forecasting period and high accuracy [9], [10], [11], [12]. Statistical models can be divided into monolithic and hybrid models. Support vector machines (SVMs) classify and regress samples by finding the optimal classification hyperplane satisfying constraints. SVMs have been widely used in several fields, including flood forecasting; however, SVM models are more sensitive to the choice of parameters and kernel functions [13]. Long and short term memory neural networks (LSTM) are widely used for flood forecasting by continuously storing useful information by memory neurons for time series prediction. However, the choice of hyperparameters for LSTM models has a large impact on the prediction performance of the models [14], [15]. Monolithic models usually have the problems of poor generalization ability and low prediction accuracy, and hybrid models can effectively solve the limitations of monolithic models. For example, using discrete wavelet transform (DWT) to extract signal features and then simulating the flood process by LSTM can effectively reduce the prediction error of the model and improve the accuracy of flood prediction. However, the choice of wavelet basis has a large impact on the results and is not suitable for the decomposition of non-smooth signals [16]. Unlike DWT, empirical mode decomposition (EMD) performs particularly well in dealing with nonlinear and non-stationary signals [17]. Combining EMD and SVM to construct an EMD-SVM model and applying it to regional runoff prediction can effectively improve the prediction accuracy of SVM. The results show that the EMD-SVM hybrid model can effectively improve the accuracy of runoff prediction [18]. The accuracy of flood forecasting can be significantly increased by combining variational mode decomposition (VMD) with least squares support vector regression (LSSVR) [19] and LSTM [20]. However, EMD suffers from mode mixing problems, and both ensemble empirical mode decomposition (EEMD) and adaptive white noise overall empirical mode decomposition (CEEMDAN) mitigate the mode mixing problem of EMD during decomposition by introducing noise-assisted analysis methods [21], [23]. In contrast to the EMD-like method, VMD uses the alternating multiplier method to tackle the variational problem without a mode mixing issue [24]. Combining the VMD algorithm with the slope entropy (SloE) method, a model based on VMD and SloE is proposed for the analysis of hydroacoustic signals. The VMD is first used to decompose the hydroacoustic signal into a series of intrinsic mode functions, and then the recognition rate is calculated by the k-nearest neighbour (KNN) algorithm. The results show that the recognition rate of the hybrid method of SloE and VMD is the highest under single feature conditions [25]. The VMD method is used to decompose the original signal, and the two-way long and short term memory network (BILSTM) is used to predict the decomposed signal. The results show that the VMD method can effectively reduce the non-stationary characteristics of the original signal, thus improving the prediction accuracy of the model [26]. Fusing VMD with a least squares support vector machine model can effectively improve the prediction of the model. First, the original signal is decomposed using the vmd method. For each component, a least squares support vector machine is used for prediction separately; finally, the prediction results of each sub-series are superimposed and reconstructed to obtain the final prediction value. The experimental results show that the prediction results obtained based on this method have higher accuracy [27].

On this basis, this study proposes a broad learning (BL) model based on improved variational mode decomposition (VMD), and applies it to regional flood prediction. Firstly, the regularised broad learning (RBL) is improved using orthogonal triangular decomposition (QR) and forgetful online sequence learning mechanism (FOS) to construct a FOS-QR-RBL model to improve the computational efficiency and generalisation capability of the BL model. Then, the endpoint effect of VMD is solved by grey correlation analysis, and the parameters of VMD are determined by particle swarm algorithm. Finally, based on the ''decomposition-synthesis-prediction'' strategy, the improved VMD is combined with the FOS-QR-RBL to build an improved VMD-FOS-QR-RBL flood prediction model, which can effectively improve the accuracy and reliability of flood prediction, and thus enhance the capability and efficiency of regional disaster prevention and mitigation.

The rest of the paper is organized as follows. Section 2 presents the relevant theory, Section 3 focuses on the model construction, Section 4 presents the experimental results and analysis, and Section 5 focuses on the conclusions and future prospects of the study.

II. CORRELATION THEORY

A. FOS-QR-RBL

The broad learning model (BL) was proposed by Chen et al. [28] in 2018. The training process of the BL model does not require repeated iteration of samples, so compared with traditional backpropagation neural networks and deep neural networks, BL has the advantages of simple structure and accurate modeling [29]. FOS-QR-RBL first introduces regularization items on the basis of BL model [30], then uses QR decomposition to redefine the output of the BL enhancement layer [31], and finally introduces an online sequence learning and forgetting mechanism. Compared with the traditional BL model, FOS-QR-RBL has the advantages of simple calculation structure, short training time and strong generalization ability [32]. Figure 1 shows the topology of the broad learning model.

For any given training sample X, Y, after n groups of feature mapping, the feature matrix Z^n can be defined as formula (1):

$$Z_i = \sigma\left(XW_{ei} + \beta_{ei}\right), \quad i = 1, 2, \ldots, n \tag{1}$$

where $X \in R^{N\times M}$, N is the number of input samples, M is the dimensionality of each sample, W_{ei} and β_{ei} are the

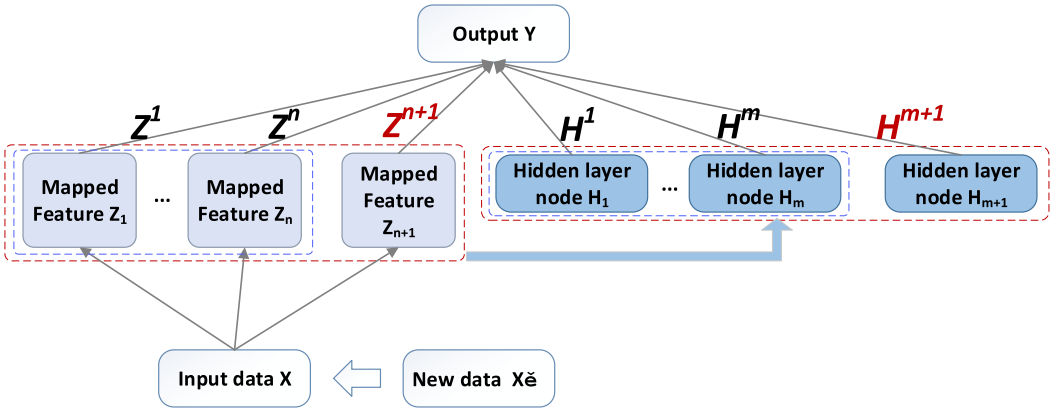

FIGURE 1. Topological structure of broad learning model.

enhancement layer weight and bias, respectively; σ is the activation function.

Then connect Z^n to the enhancement layer node for nonlinear transformation. The output matrix H^m of the j-th group of enhanced nodes can be defined as formula (2):

$$H_j = \xi\left(Z^n W_{hj} + \beta_{hj}\right), j = 1, 2 \ldots, m \tag{2}$$

where, ξ is the activation function of the enhancement layer and W_{hj} and β_{hj} are the output weight and bias terms of the enhancement layer, respectively. Therefore, the final output of BL can be defined as follows:

$$Y = (Z_1, Z_2, \ldots, Z_n, H_1, H_2, \ldots, H_m)\, W = (Z^n, H^m)W \tag{3}$$

where $Y \in R^{N\times C}$, C is the dimensionality of the corresponding output and W is the weight connecting the feature node layer and the enhanced node layer to the output layer, which can be obtained by calculating the ridge regression of (Z^n, H^m) and Y [33], [34], [35], [36], [37].

$$W = (Z^n, H^m)^+ Y \tag{4}$$

The standard BL model is based on the principle of empirical risk minimization, and the training process is prone to overfitting. Regularization theory effectively solves this problem [38]. The mathematical model of regularized broad learning (RBL) can be expressed as:

$$W = \left(Z^n, H^m\right)^T \left[\left(Z^n, H^m\right)\left(Z^n, H^m\right)^T + \frac{I}{C}\right]^+ Y \tag{5}$$

Among them, C is the regularization coefficient, and I is the sample size [39], [40].

In the process of determining the output of the RBL enhancement layer, QR decomposition is used to redefine the $\left[(Z^n, H^m)(Z^n, H^m)^T + \frac{I}{C}\right]^+$ solution scheme. Compared with the standard RBL model, QR-RBL has the advantages of simple calculation structure and fast convergence speed [41], [42]. Among them, the output of the enhancement layer of QR-RBL is defined as follows.

$$\begin{aligned} E^+ &= R_{l+1}^{-1} Q_{l+1}^T \\ &= \begin{bmatrix} R_l^{-1} & -R_l^{-1} r_{l+1} r_{l+1,l+1}^{-1} \\ 0 & r_{l+1,l+1}^{-1} \end{bmatrix} \begin{bmatrix} Q_l^T \\ q_{l+1}^T \end{bmatrix} \\ &= \begin{bmatrix} f_l - R_l^{-1} r_{l+1} f_{l+1}^T \\ f_{l+1}^T \end{bmatrix} \end{aligned} \tag{6}$$

where, Q is the orthogonal matrix and R is the upper triangular matrix; $E^+ = \left[(Z^n, H^m)(Z^n, H^m)^T + \frac{I}{C}\right]^+$ is the output of the enhancement layer [43], [44], [45].

Forgetting mechanism is an effective method to gradually remove obsolete information and error data. Reference [46] combined forgetting mechanism in OS-ELM algorithm and proposed forgetting mechanism FOS-ELM algorithm. In this paper, we introduce the forgetting mechanism into OS-QR-RBL and propose the online sequence broad learning FOS-QR-RBL method based on the forgetting mechanism, so that OS-QR-RBL can effectively remove the error information and obsolete information data. FOS-QR-RBL is mainly divided into two parts. The first part initializes the output weight W with a small number of training samples; the second part is the online learning stage [47]. When a new sample is input, the weights W, P of the new sample in the hidden layer are obtained recursively, and the k-th iteration calculates the definition of W^k as follows:

$$W^k = W^{k-1} + P_k E_k^T \left[Y_k - E_k W^{k-1}\right] \tag{7}$$

where P_k is defined as formula (8):

$$P_k = P_{k-1} - P_{k-1} E_k^T \left(I_u + E_{k-1} P_{k-1} E_k^T\right)^{-1} E_k P_{k-1} \tag{8}$$

where I_u is the identity matrix [48], [49], [50].

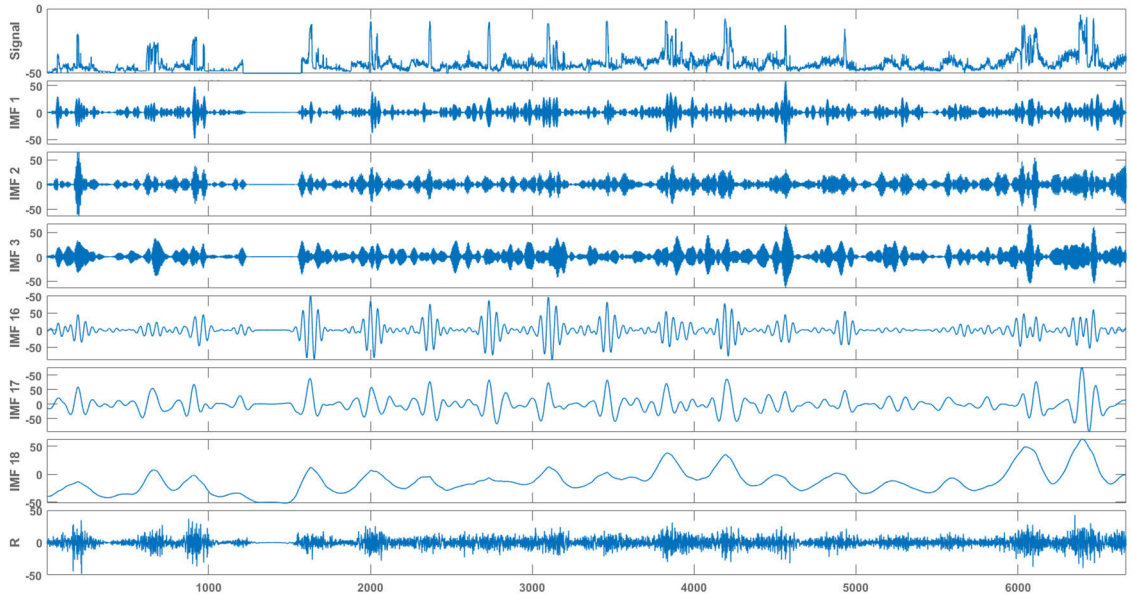

FIGURE 2. VMD decomposition of original runoff series.

B. VMD

VMD is an adaptive and completely non-recursive mode variation and signal processing technology, which overcomes the problem of mode component aliasing existing in the empirical mode decomposition method and has a more solid mathematical theoretical foundation [51], [52]. Figure 2 shows the decomposition effect of the VMD method on the original runoff series, where signal is the original waveform, IMFi is the i^{th} component signal, and R is the residual component, and its implementation can be described as follows:

For a given sample X, the variational problem is described as using the centre frequency to solve the mode function $u_k(t), k = 1, 2, \ldots, k$ to minimize the sum of bandwidth estimates for each mode. The sum of all mode functions is equal to the original sample X, and the specific expression is as follows:

$$\min_{\{u_k\},\{\omega_K\}} \left\{ \sum_{k=1}^{k} \left\| \partial_t \left[\left(\delta(t) + \frac{j}{\pi t} \right) u_k(t) \right] e^{-j\omega_k t} \right\|_2^2 \right\}$$
$$\text{s.t.} \left\{ \sum_{k=1}^{k} u_k = X \right\} \tag{9}$$

where $\{u_k\} = \{u_1, u_2, \ldots, u_k\}$ represents the K eigenmode components (IMF) obtained by decomposition; $\{\omega_k\} = \{\omega_1, \omega_2, \ldots, \omega_k\}$ represents the centre frequency of the component; $\otimes$ is the convolution calculation, K is the total number of mode functions, $\delta(t)$ is the Dirac distribution, and $e^{-j\omega_k t}$ is the centre frequency of the mode function on the complex plane, where K is the centre frequency of the mode function.

To obtain the optimal solution of the above constraint variables, the secondary penalty factor α and Lagrange multiplication operator $\lambda(t)$ are introduced. The secondary penalty factor is used to ensure the reconstruction accuracy of the signal in the presence of Gaussian noise, and the Lagrange operator is to maintain the constraint conditions as strict, and are defined as follows:

$$\begin{aligned} L(\{u_k\}, \{\omega_k\}, \lambda) = & \\ & \times \left\langle \lambda(t), f_{Runoff}(t) - \sum_k u_k(t) \right\rangle \\ & + \left\| f_{Runoff}(t) - \sum_k u_k(t) \right\|_2^2 \\ & + \alpha \sum_k \left\| \partial_t \left[\left(\delta(t) + \frac{j}{\pi t} \right) * u_k(t) \right] e^{-j\omega_k t} \right\|_2^2 \end{aligned} \tag{10}$$

In the formula, the iterative terms $\{u_k\}, \{\omega_k\}$ and λ use the alternating direction multiplier method to obtain the saddle point of the augmented Lagrangian expression through iterative updating [53],[54], [55], [56], [57], [58], [59], [60], [61].

III. CONSTRUCTION OF THE FLOOD FORECASTING MODEL

A. END EFFECT IMPROVEMENT SCHEME BASED ON THE GREY RELATIONAL ANALYSIS

VMD uses the local extrema of the original signal to obtain the envelope estimation function, and then obtains each IMF component. Since it is impossible to accurately determine whether the endpoint is a maximum value or a minimum value, there is an error in obtaining the envelope estimation function, which makes the IMF component lose its physical meaning. At present, the main solution to the end effect is to extend the signal at both ends, such as the correlation

wave extension method, the mirror image extension method, and the extreme value extension method. This study is based on grey relational analysis to extend the original signal to improve the end effect of VMD. The basic realization is as follows.

Suppose the maximum value sequence of the original signal $\mathbf{x(t)}$ is $\mathbf{M(i)}, \mathbf{i = 1, 2, \ldots, n}$, and the minimum value sequence is $\mathbf{N(j)}, \mathbf{j = 1, 2, \ldots, m}$. Assuming that the first extreme point of the left end point is a maximum value, the waveform from the left end point $\mathbf{x(0)}$ to the first extreme point $\mathbf{M(0)}$ is taken as the research object, which is defined as $\mathbf{W_0}$.

Take $\mathbf{M(i)}$ as the corresponding point of $\mathbf{M(0)}$ respectively and intercept the wavelet $\mathbf{W_i}$ of the same length as $\mathbf{W_0}$. Standardize $\mathbf{W_0}$ and $\mathbf{W_i}$ respectively, where the standardization equation is defined as follows.

$$W_i' = \frac{W_i(k)}{W_i(0)}, k = 1, 2, \ldots, l \tag{11}$$

3) Calculate the gray correlation coefficient $\boldsymbol{\eta_{W_0W_i}(k)}$ between $\mathbf{W_0}$ and $\mathbf{W_i}$, as in (12), shown at the bottom of the page.

Among them, $\boldsymbol{\rho \in (0, 1)}$ is the resolution coefficient, which is usually 0.5. When $\boldsymbol{\eta_{max}(k) = \eta_{W_0W_i}(k)}$ is assumed, several sub-signals before $\mathbf{W_i}$ are extended to the left end of the original signal.

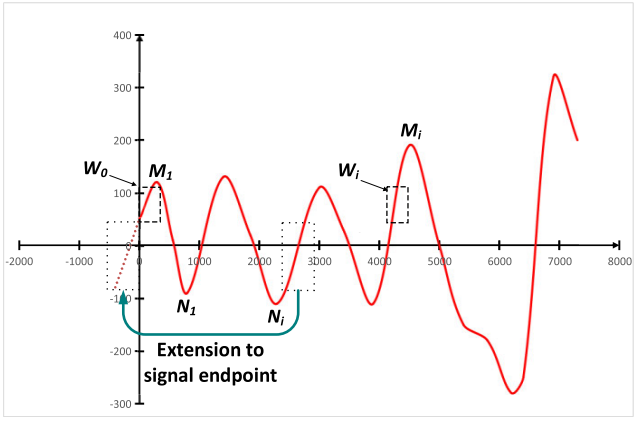

FIGURE 3. Schematic diagram of VMD endpoint extension.

Extend the right end of the original signal in the same way, then perform VMD decomposition on the extended signal, and intercept each component according to the time corresponding to x(t) to obtain a VMD decomposition result that improves the end effect. Figure 3 shows the schematic diagram of VMD endpoint extension.

B. OPTIMIZATION OF VMD BY PARTICLE SWARM OPTIMIZATION

VMD has better decomposition effect on complex data, strong resistance to noise interference, and higher accuracy of decomposition results. However, VMD needs to pre-set two parameters of bandwidth limit α and number of decomposition k. Therefore, the article adopts particle swarm optimization algorithm (PSO) to optimize the parameters of VMD and introduces fuzzy entropy as the fitness function of particle swarm to optimize the parameters of VMD for calculation [62], [63]. The fuzzy entropy can measure the complexity of the time series, and the larger fuzzy entropy represents the higher complexity of the series, and the opposite is the lower complexity of the series. The overall flow of the vmd parameter optimization is given in Figure 4 and the basic idea is as follows:

$$FE(m, n, r) = \lim_{N\to\infty}\left[\ln \frac{\emptyset^m(n, r)}{-} \ln \emptyset^{m+1}(n, r)\right] \tag{13}$$

1) Initialise the parameters of PSO by setting the population size N to 30, the inertia factor w to 0.5, the learning factors c_1 and c_2 to 0.5 respectively, the maximum number of iterations t to 50, the position and velocity to random values, and the fuzzy entropy $FE(m, n, r)$ as the fitness function of the particle swarm algorithm, defined as follows.

where m, n and r represent the window size, boundary gradient and width respectively. $\emptyset$ is the affiliation function.

2) Randomly generate the particle position (k, α) and particle velocity V_{id} in the particle population, then use VMD to decompose the original data and calculate the fuzzy entropy value corresponding to each particle position for the signal at different particle positions (k, α).

3) The size of the fuzzy entropy $FE(m, n, r)$ is updated by constantly comparing it with the size of the fuzzy entropy $FE(m, n, r)$, so that the individual extremes and the global extremes are optimal. The particle population consists of n particles in d-dimensional space, and the position of the ith particle is denoted as $X_i = (x_{i1}, x_{i2}, \ldots, x_{id}), i = 1, 2, \ldots, n$; the velocity of the ith particle is $V_i = (v_{i1}, v_{i2}, \ldots, v_{id}), v = 1, 2, \ldots, n$; the optimal solution searched by the ith particle is noted as: $P_{best} = (P_{i1}, P_{i2}, \ldots, P_{id})$; the global optimal solution for the whole population is: $g_{best} = (P_{g1}, P_{g2}, \ldots, P_{gd})$; and the particle velocity and position updates are given by:

$$V_{id}^{t+1} = W^t \times V_{id}^t + C_1 r_1 \left(P_{id}^t - X_{id}^t\right) + C_2 r_2 \left(P_{gd}^t - X_{gd}^t\right) \tag{14}$$

$$X_{id}^{t+1} = X_{id}^t + V_{id}^{t+1} \tag{15}$$

$$\eta_{W_0W_i}(k) = \frac{1}{n}\sum_{k=1}^{1} \frac{\min\min|W_0(k) - W_i(k)| + \rho\max\max|W_0(k) - W_i(k)|}{|W_0(k) - W_i(k)| + \rho\max\max|W_0(k) - W_i(k)|} \tag{12}$$

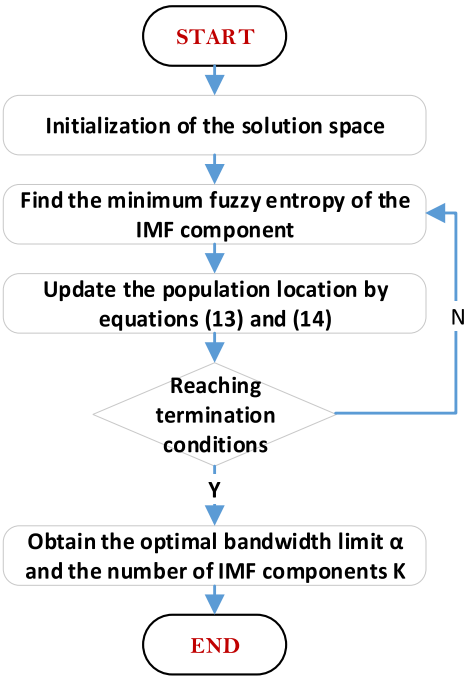

FIGURE 4. Flow chart of the PSO-VMD algorithm.

where t is the current number of iterations; r_1 and r_2 are uniformly distributed random numbers, and c_1 and c_2 are acceleration constants.

4) Loop steps 2 to 3, ending the loop when the number of iterations reaches a preset maximum, resulting in the optimal number of decomposition layers and penalty factor (k, α).

C. CONSTRUCTION OF PARALLEL IMPROVED VMD-FOS-QR-RBL METHOD

By fusing the improved VMD with the FOS-QR-nRBL model, a flood forecasting model based on the ''decomposition-synthesis'' strategy (improved VMD-FOS-QR-RBL model) is proposed. The flow chart of Improved VMD-FOS-QR-RBL model construction is shown in Figure 5, and its basic realization is as follows:

1) Taking the Xiaolangdi Reservoir in the Yellow River Basin as the experimental object, collect the runoff data of Xiaolangdi Reservoir in real-time and perform data cleaning work such as missing value filling, field deduplication and outlier processing, and normalizing the clean data. The normalization function is defined as follows:

$$X^* = \frac{X - \min(X)}{\max(X) - \min(X)} \tag{16}$$

where $\max(X)$ is the maximum value of the sample and $\min(X)$ is the minimum value of the sample.

2) After the data is normalized, the boundary is extended first, and then the extended data is used to initialize and optimize the vmd related parameters, which mainly include balance parameters, noise tolerance, optimal mode number, and initialized centre frequency. The optimization equation is defined as follows:

$$J(\theta) = \frac{1}{2}\sum_{i=1}^{m} h_\theta\left(x^i\right) - y^i, J_\theta \tag{17}$$

where $h(x)$ represents the reconstruction data after VMD decomposition, and y represents the true value. According to the PSO-VMD algorithm, the balance parameters, noise tolerance, optimal mode number, and initialized centre frequency were set to 8605, 0, 18, and 1, respectively.

The final decomposition results are obtained by intercepting the boundary positions that correspond to the original signal after the VMD decomposition. The training set, which makes up 65% of the data for each IMF component, and the test set, which makes up 35% of the data, are both inputs to the model. Finally, the historical samples from the previous n days are used as input, and the samples from the predicted n+m days are used as output. The prediction results from the individual components are then added together to produce the final prediction results.

4) The flood control operation of reservoirs and hydrological stations can be briefly described as finding the optimal control plan for each reservoir according to its storage capacity and inflow process during the operation period. To satisfy various constraints, the flood process through the downstream flood control point of the reservoir should be as flat as possible and the peak discharge should be as small as possible. The objective function can be expressed as

$$F_{min} - Min\sum_{t=1}^{T} Q_t^2 = Min\sum_{t=1}^{T}\left(\sum_{i=1}^{N} R_{i,t-\tau_i}\right)^2 \tag{18}$$

where $F_{\min}$ is the flood control benefit; Q_t is the flood flow at the flood control point C during the t period; T is the total number of periods; and $R_{i,t-\tau_i}$ is the outflow flow of the i reservoir during the $i-\tau_i$ period.

D. MODEL EVALUATION

The Nash–Sutcliffe coefficient (E_{ns}), mean absolute error (MAE), relative error (RE), and run time were selected as evaluation criteria in the validation process to comprehensively determine the algorithm's reliability, stability, accuracy, and execution efficiency. The E_{ns} was used to evaluate the reliability of the prediction model. Its value range is $(-\infty, 1]$; when E_{ns} is close to 1, the overall results are credible, but the process simulation error is large. When E_{ns} is significantly below 0, the model is not credible. The RE and MAE are used to evaluate the real-time error and overall error, respectively. Definition of each indicator is as follows:

$$E_{ns} = 1 - \left[\frac{\sum_{i=1}^{n}\left(Q_o - Q_f\right)^2}{\sum_{i=1}^{n}\left(Q_o - \bar{Q}_o\right)^2}\right] \tag{19}$$

$$MAE = \frac{1}{n}\sum_{i=1}^{n}\left|Q_f - Q_o\right| \tag{20}$$

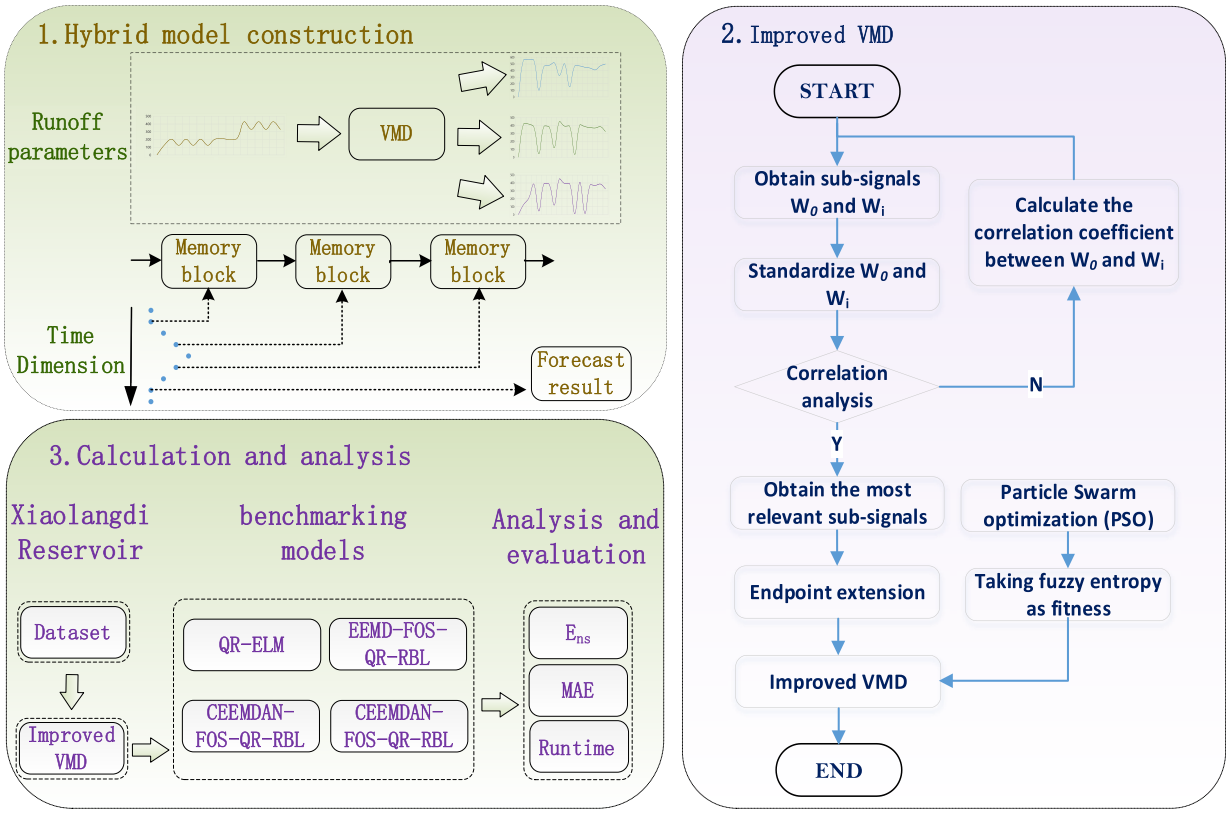

FIGURE 5. Flow chart of Improved VMD-FOS-QR-RBL model construction.

$$RE = \left(\frac{Q_o - Q_f}{Q_o}\right) * 100\% \tag{21}$$

among them $Q_o, Q_f, \bar{Q}_o, \bar{Q}_f$, are the observed value, predicted value, average observed value, and average predicted value, respectively.

IV. RESULTS AND ANALYSIS

Xiaolangdi Reservoir is the only integrated water conservancy hub that can control the downstream runoff of the Yellow River, which has superior natural conditions and a significant strategic position, out of the 32 hydrological stations in the Yellow River basin. In a 390,000 data set, the daily observed runoff data from Xiaolangdi and Tongguan hydrological stations are used to test the model's applicability and robustness. The results of the prediction curves are displayed in Figure 6 and the article uses the benchmark models QR-ELM, EEMD-FOS-QR-RBL, and CEEMDAN-FOS-QR-RBL for comparison and validation.

The prediction curves for the observed value curve, EEMD-FOS-QR-RBL, CEEMDAN-FOS-QR-RBL, QR-ELM, and the improved VMD-FOS-QR-RBL model are shown in Fig. 6 in the colours red, blue, green, purple, and orange, respectively. Figures 6(a) and 6(b) show the results of the Xiaolangdi hydrological station's prediction for the next one and seven days, while Figures 6(c) and 6(d) show the results of the Tongguan hydrological station's prediction for the same time periods. As can be seen from the figure, the performance of the VMD-FOS-QR-RBL and CEEMDAN-FOS-QR-RBL models is similar for low latency future forecasts, but as the number of forecast days increases, the VMD-FOS-QR-RBL has higher accuracy relative to the CEEMDAN-FOS-QR-RBL and EEMD-FOS-QR-RBL, QR-ELM was the least effective, due to the fact that the VMD method is effective in improving the robustness and generalization of the broad learning model. In addition. Fixing the number of future days and adjusting the features and sequence length of the predicted sequence, VMD-FOS-QR-RBL is highly stable compared to other models.

Figure 7 provides the box plots of the model's relative errors at the two hydrological stations. The relative errors for forecasting the Xiaolangdi hydrological station for the following one and seven days are shown in Figures 7(a) and 7(b), while the relative errors for forecasting the Tongguan hydrological station for the following one and seven days are shown in Figures 7(c) and 7(d). The median error is indicated by the solid line in the centre of the box, and the dashed line in the figure represents the mean value of the errors. As can be seen from the graph, the VMD-FOS-QR-RBL model has an error interval, median and mean error within 0.5 overall, followed by the FOS-QR-RBL model, which is within 3.5 overall. The errors of the FOS-QR-RBL coupled EEMD and CEEMDAN are larger when the prediction period is short, and the relative errors gradually decrease as the prediction period increases. The

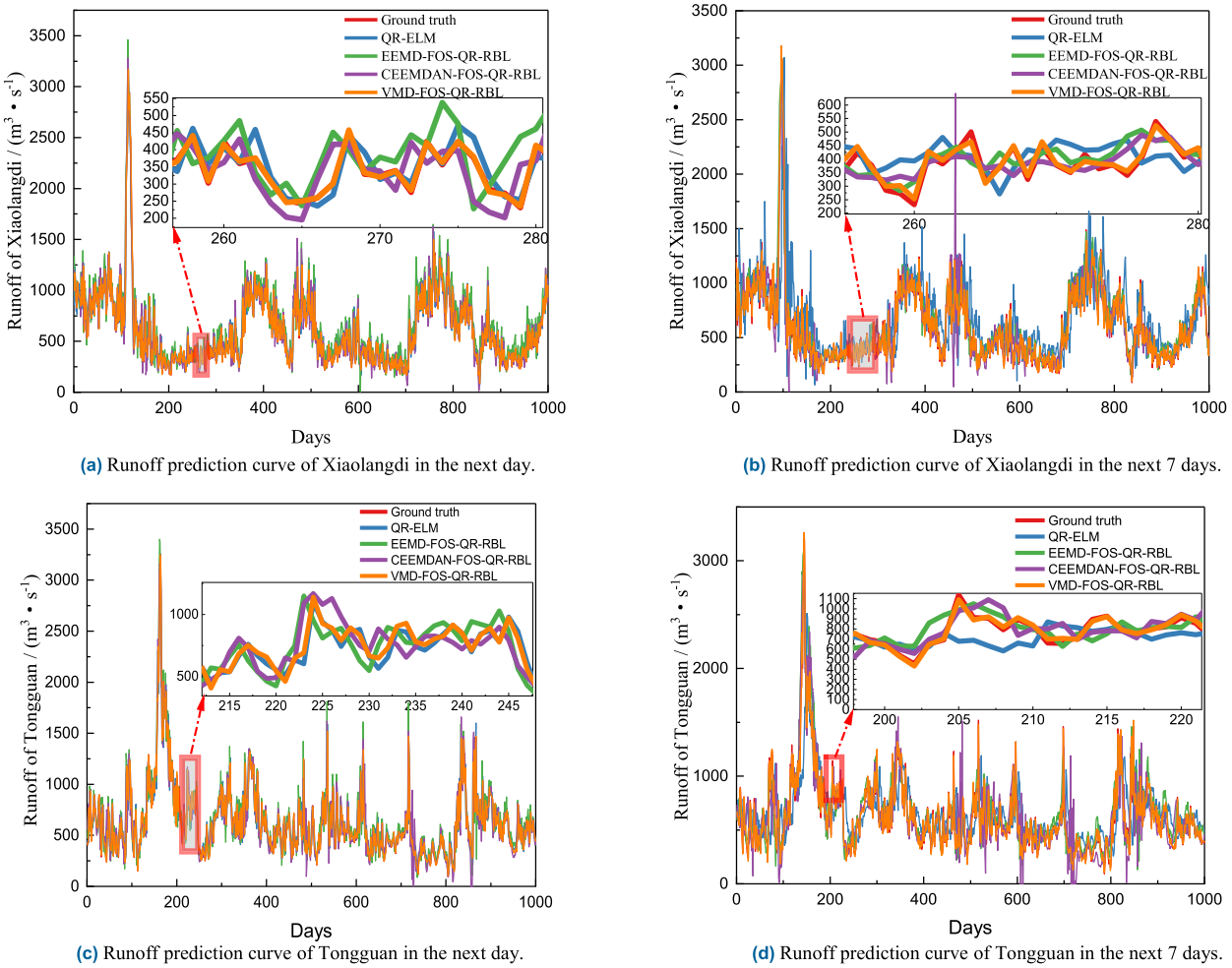

(a) Runoff prediction curve of Xiaolangdi in the next day.

(b) Runoff prediction curve of Xiaolangdi in the next 7 days.

(c) Runoff prediction curve of Tongguan in the next day.

(d) Runoff prediction curve of Tongguan in the next 7 days.

FIGURE 6. Runoff prediction curves of different models at different hydrological stations.

VMD-FOS-QR-RBL model, on the other hand, has a smaller overall prediction error, higher accuracy and is more stable compared to the other models. Due to the mode confounding and endpoint effects of the EEMD and CEEMDAN methods, the model suffers from signal distortion during non-stationary signal processing, which affects the prediction accuracy.

To verify the validity and stability of the models, 50 Monte Carlo simulations were conducted for each model in this paper, using different input data as variables. The mean statistic reflects the average level of the model predictions, and the variance statistic reflects the degree of bias of the model predictions. the lower the mean value of MAE and the higher the mean value of E_{ns}, the better the average level of the model predictions, and the lower the variance indicates that the model predictions are more stable. The means and variances of MAE and E_{ns} predicted by different models at different time levels are shown in Table 1. Compared to the EEMD-FOS-QR-RBL and CEEMDAN-FOS-QR-RBL models, the improved VMD-FOS-QR-RBL predicted 80.30% and 84.10% lower mean values for MAE, 15.51% and 28.16 higher mean values for E_{ns}, and 99.72% and 99.60% lower variances for MAE, respectively. It shows that the improved VMD method has higher non-stationary handling and signal analysis capability compared to EEMD and CEEMDAN, and is better able to improve the validity and stability of the FOS-QR-RBL model prediction.

The running times of the FOS-QR-RBL model proposed in the article and the conventional broad learning model are given in Table 2. Compared with RBL and QR-RBL, the running efficiency of the FOS-QR-RBL model improved by 35 and 23.68%, respectively, indicating that the incorporated online sequence forgetting mechanism can effectively improve the running efficiency of the model.

The reconstruction error of the improved VMD method based on grey correlation analysis is given in Table 3, and the results show that the reconstruction error of the improved VMD is reduced by 94.71%. The grey correlation analysis method effectively mitigates the endpoint effect of the VMD method by broadening the original signal and reduces the reconstruction error.

TABLE 1. Comparison of the numerical results for various evaluation indicators.

Foresigh t period	Model	past 7 days predicting future 1 day	past 14 days predicting future 1 day	Past 21 days predicting future 1 day	past 28 days predicting future 1 day	past 14 days predicting future 7 days	past 21 days predicting future 7 days	past 28 days predicting future 7 days	past 35 days predicting future 7 days
Mean value of MAE	QR-RBL	127.84	192.80	199.41	185.37	317.43	371.40	312.14	289.38
	FOS-QR-RBL	151.27	200.41	217.11	196.54	327.44	386.77	330.43	305.91
	QR-ELM	98.6	101.88	112.51	114.01	165.16	165.93	166.08	166.41
	EEMD-FOS-QR-RBL	72.28	56.06	59.48	84.17	108.26	117.38	124.74	134.26
	CEEMDAN-FOS-QR-RBL	60.65	74.68	80.31	84.06	138.72	168.12	158.63	172.27
	improved VMD-FOS-QR-RBL	3.83	3.66	3.89	3.82	30.05	30.57	32.89	40.38
Mean value of E_{ns}	QR-RBL	0.41	0.00	0.04	0.14	-0.84	-1.44	-0.56	-0.25
	FOS-QR-RBL	0.09	-0.06	-0.08	0.09	-1.04	-1.46	-0.69	-0.32
	QR-ELM	0.45	0.41	0.39	0.38	0.20	0.20	0.21	0.21
	EEMD-FOS-QR-RBL	0.47	0.46	0.46	0.41	0.34	0.29	0.28	0.23
	CEEMDAN-FOS-QR-RBL	0.47	0.41	0.42	0.42	0.32	0.19	0.17	0.10
	improved VMD-FOS-QR-RBL	0.50	0.50	0.50	0.50	0.37	0.37	0.38	0.36
Variance of MAE	QR-RBL	22637.68	37189.86	39823.11	34393.04	100872.56	138182.08	97704.79	83858.96
	FOS-QR-RBL	22883.58	40164.37	47137.34	38628.24	107222.81	149592.60	109189.90	93582.74
	QR-ELM	9843.03	10518.46	12807.11	13226.27	28102.91	28246.37	28333.31	28397.17
	EEMD-FOS-QR-RBL	5224.80	3209.51	3590.11	7152.78	11804.01	13837.14	15615.84	18099.63
	CEEMDAN-FOS-QR-RBL	3679.13	5620.68	6491.10	7128.94	19252.96	24827.62	25284.96	29982.83
	improved VMD-FOS-QR-RBL	14.74	13.41	15.27	14.78	959.36	970.14	1112.94	1976.77
Variance of E_{ns}	QR-RBL	0.00	0.00	0.00	0.02	0.71	2.09	0.32	0.06
	FOS-QR-RBL	0.01	0.00	0.01	0.00	1.08	2.13	0.47	0.10
	QR-ELM	0.17	0.16	0.15	0.15	0.04	0.04	0.04	0.04
	EEMD-FOS-QR-RBL	0.22	0.21	0.21	0.17	0.12	0.09	0.08	0.07
	CEEMDAN-FOS-QR-RBL	0.22	0.17	0.17	0.18	0.10	0.04	0.04	0.04
	improved VMD-FOS-QR-RBL	0.25	0.25	0.24	0.25	0.14	0.14	0.14	0.13

The combined results shown in Figures 6 and 7, Tables 1 and 3 show that the improved VMD-FOS-QR-RBL model exhibits better prediction results compared to the other benchmark models because the online sequence forgetting mechanism and the improved VMD method effectively improve the accuracy and robustness of the FOS-QR-RBL model predictions. Compared with the unimproved VMD-LSTM model, the improved VMD-FOS-QR-RBL model exhibited higher accuracy, confidence, and smaller error in the prediction results at different time scales.

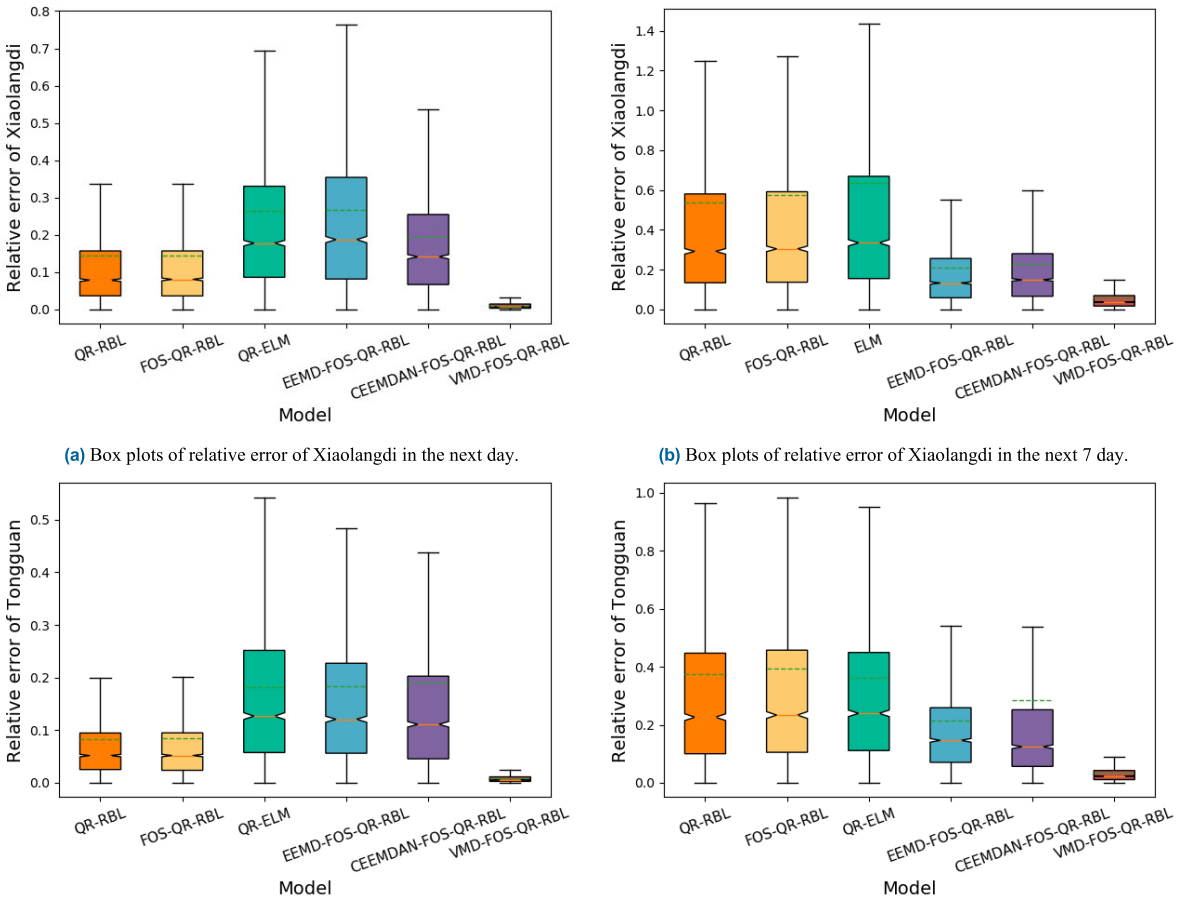

(a) Box plots of relative error of Xiaolangdi in the next day.

(b) Box plots of relative error of Xiaolangdi in the next 7 day.

(c) Box plots of relative error of Tongguan in the next day.

(d) Box plots of relative error of Tongguan in the next 7 days.

FIGURE 7. Box plots of relative error of different models at different hydrological stations.

TABLE 2. Comparison of the computing time of various models.

Model	Data preprocessing time (s)	Calculation and prediction time (s)
RBL	0	2.440
QR-RBL	0	2.078
FOS-QR-RBL	0	1.586
VMD-FOS-QR-RBL	7.038	0.062

TABLE 3. Comparison of the computing time of various models.

Scenes	Reconstruction error
Endpoint extreme value unknown	21.373
Extremum Extension Based on Grey Relation Analysis	403.907

V. CONCLUSION

We propose an improved parallel VMD-FOS-QR-RBL-based flood forecasting model based on the ''decomposition-synthesis-forecasting'' strategy, using forgetting online sequences, QR decomposition, and parallel computing to improve the forecasting accuracy and computational efficiency of the broad learning model, and using grey correlation analysis to suppress the endpoint effect of VMD to overcome the problems of low accuracy, poor credibility, and low efficiency in flood forecasting. The experimental results show that the improved parallel VMD-FOS-QR-RBL model proposed in this paper has a high degree of generalisation and robustness for various prediction steps. Although parallel computing can effectively improve the computational efficiency of the model, the addition of the VMD method and optimization algorithm requires the model's overall computational efficiency to be improved further.

REFERENCES

[1] X. Huang, B. Xu, P.-A. Zhong, H. Yao, H. Yue, F. Zhu, Q. Lu, Y. Sun, R. Mo, Z. Li, and W. Liu, "Robust multiobjective reservoir operation and risk decision-making model for real-time flood control coping with forecast uncertainty," *J. Hydrol.*, vol. 605, Feb. 2022, Art. no. 127334.

[2] Z. Jiang, S. Yang, Z. Liu, Y. Xu, Y. Xiong, S. Qi, Q. Pang, J. Xu, F. Liu, and T. Xu, "Coupling machine learning and weather forecast to predict farmland flood disaster: A case study in Yangtze river basin," *Environ. Model. Softw.*, vol. 155, Sep. 2022, Art. no. 105436.

[3] B. El Fathi, F. El Hassani, M. Moukhliss, N. Mazigh, A. Dra, A. Ouallali, A. Kherbeche, and A. Taleb, "Flood forecast and flood vulnerability modeling in case of Wadi Fez, Morocco," *Arabian J. Geosci.*, vol. 15, no. 6, pp. 1–24, Mar. 2022.

[4] T. Lopez et al., "On the use of satellite remote sensing to detect floods and droughts at large scales," *Surv. Geophys.*, vol. 41, no. 6, pp. 1461–1487, 2020, doi: 10.1007/s10712-020-09618-0.

[5] F. Chen, J. Chen, and J. Liu, "Forecast of flood disaster emergency material demand based on IACO-BP algorithm," *Neural Comput. Appl.*, vol. 34, no. 5, pp. 3537–3549, Mar. 2022.

[6] L. L. Moreira, M. M. de Brito, and M. Kobiyama, "A systematic review and future prospects of flood vulnerability indices," *Natural Hazards Earth Syst. Sci.*, vol. 21, no. 5, pp. 1513–1530, 2021, doi: 10.5194/nhess-21-1513-2021.

[7] B. Hadid, E. Duviella, and S. Lecoeuche, "Data-driven modeling for river flood forecasting based on a piecewise linear ARX system identification," *J. Process Control*, vol. 86, pp. 44–56, Feb. 2020.

[8] B. T. Pham, M. Avand, S. Janizadeh, T. V. Phong, N. Al-Ansari, L. S. Ho, S. Das, H. V. Le, A. Amini, S. K. Bozchaloei, F. Jafari, and I. Prakash, "GIS based hybrid computational approaches for flash flood susceptibility assessment," *Water*, vol. 12, no. 3, p. 683, Mar. 2020.

[9] X.-H. Le, H. V. Ho, G. Lee, and S. Jung, "Application of long short-term memory (LSTM) neural network for flood forecasting," *Water*, vol. 11, no. 7, p. 1387, Jul. 2019.

[10] Y. Ding, Y. Zhu, J. Feng, P. Zhang, and Z. Cheng, "Interpretable spatio-temporal attention LSTM model for flood forecasting," *Neurocomputing*, vol. 403, pp. 348–359, Aug. 2020.

[11] T. Han, Y.-F. Li, and M. Qian, "A hybrid generalization network for intelligent fault diagnosis of rotating machinery under unseen working conditions," *IEEE Trans. Instrum. Meas.*, vol. 70, pp. 1–11, 2021, doi: 10.1109/TIM.2021.3088489.

[12] Z. Chen, G. He, J. Li, Y. Liao, K. Gryllias, and W. Li, "Domain adversarial transfer network for cross-domain fault diagnosis of rotary machinery," *IEEE Trans. Instrum. Meas.*, vol. 69, no. 11, pp. 8702–8712, Nov. 2020, doi: 10.1109/TIM.2020.2995441.

[13] Z. Liang, Y. Li, Y. Hu, B. Li, and J. Wang, "A data-driven SVR model for long-term runoff prediction and uncertainty analysis based on the Bayesian framework," *Theor. Appl. Climatol.*, vol. 133, nos. 1–2, pp. 137–149, Jul. 2018.

[14] Z. Cui, Y. Zhou, S. Guo, J. Wang, H. Ba, and S. He, "A novel hybrid XAJ-LSTM model for multi-step-ahead flood forecasting," *Hydrol. Res.*, vol. 52, no. 6, pp. 1436–1454, Dec. 2021.

[15] Y. Xu, C. Hu, Q. Wu, S. Jian, Z. Li, Y. Chen, G. Zhang, Z. Zhang, and S. Wang, "Research on particle swarm optimization in LSTM neural networks for rainfall-runoff simulation," *J. Hydrol.*, vol. 608, May 2022, Art. no. 127553.

[16] Y. O. Ouma, R. Cheruyot, and A. N. Wachera, "Rainfall and runoff time-series trend analysis using LSTM recurrent neural network and wavelet neural network with satellite-based meteorological data: Case study of Nzoia hydrologic basin," *Complex Intell. Syst.*, vol. 8, no. 1, pp. 213–236, Feb. 2022.

[17] K. Johny, M. L. Pai, and S. Adarsh, "A multivariate EMD-LSTM model aided with time dependent intrinsic cross-correlation for monthly rainfall prediction," *Appl. Soft Comput.*, vol. 123, Jul. 2022, Art. no. 108941.

[18] M. Sibtain, X. Li, H. Bashir, and M. I. Azam, "A hybrid model for runoff prediction using variational mode decomposition and artificial neural network," *Water Resour.*, vol. 48, no. 5, pp. 701–712, Sep. 2021.

[19] G. Li, W. Chang, and H. Yang, "A novel combined prediction model for monthly mean precipitation with error correction strategy," *IEEE Access*, vol. 8, pp. 141432–141445, 2020.

[20] X. Wang, Y. Wang, P. Yuan, L. Wang, and D. Cheng, "An adaptive daily runoff forecast model using VMD-LSTM-PSO hybrid approach," *Hydrol. Sci. J.*, vol. 66, no. 9, pp. 1488–1502, Jul. 2021.

[21] E. Meng, S. Huang, Q. Huang, W. Fang, L. Wu, and L. Wang, "A robust method for non-stationary streamflow prediction based on improved EMD-SVM model," *J. Hydrol.*, vol. 568, pp. 462–478, Jan. 2019.

[22] H. Wang, J. Chen, and G. Dong, "Feature extraction of rolling bearing's early weak fault based on EEMD and tunable *Q*-factor wavelet transform," *Mech. Syst. Signal Process.*, vol. 48, nos. 1–2, pp. 103–119, Oct. 2014.

[23] S. Zhang, S.-J. Chen, G.-W. Ma, W.-B. Huang, and B. Li, "Generation hybrid forecasting for frequency-modulation hydropower station based on improved EEMD and ANN adaptive switching," *Electr. Eng.*, vol. 104, no. 5, pp. 2949–2966, Oct. 2022.

[24] L. Lv, Z. Wu, J. Zhang, L. Zhang, Z. Tan, and Z. Tian, "A VMD and LSTM based hybrid model of load forecasting for power grid security," *IEEE Trans. Ind. Informat.*, vol. 18, no. 9, pp. 6474–6482, Sep. 2022.

[25] Y. Li, B. Tang, and Y. Yi, "A novel complexity-based mode feature representation for feature extraction of ship-radiated noise using VMD and slope entropy," *Appl. Acoust.*, vol. 196, Jul. 2022, Art. no. 108899.

[26] R. Gong, J. Li, and C. Wang, "Remaining useful life prediction based on multisensor fusion and attention TCN-BiGRU model," *IEEE Sensors J.*, vol. 22, no. 21, pp. 21101–21110, Nov. 2022.

[27] C. Ding, Q. Ding, L. Feng, and Z. Wang, "Prediction model of dissolved gas in transformer oil based on VMD-SMA-LSSVM," *IEEJ Trans. Electr. Electron. Eng.*, vol. 17, no. 10, pp. 1432–1440, Oct. 2022.

[28] C. L. P. Chen and Z. L. Liu, "Broad learning system: An effective and efficient incremental learning system without the need for deep architecture," *IEEE Trans. Neural Netw. Learn. Syst.*, vol. 29, no. 1, pp. 10–24, Jan. 2018.

[29] Z. Liu and C. L. P. Chen, "Broad learning system: Structural extensions on single-layer and multi-layer neural networks," in *Proc. Int. Conf. Secur., Pattern Anal., Cybern. (SPAC)*, Dec. 2017, pp. 136–141.

[30] W. Sun and Y. Wang, "Prediction and analysis of CO_2 emissions based on regularized extreme learning machine optimized by adaptive whale optimization algorithm," *Polish J. Environ. Stud.* vol. 30, no. 3, pp. 2755–2767, 2021.

[31] Y. Liu and L. Wang, "Drought prediction method based on an improved CEEMDAN-QR-BL model," *IEEE Access*, vol. 9, pp. 6050–6062, 2021.

[32] J. Zhang, Y. Li, and W. Xiao, "Adaptive online sequential extreme learning machine for dynamic modeling," *Soft Comput.*, vol. 25, no. 3, pp. 2177–2189, Feb. 2021.

[33] S. Feng and C. L. P. Chen, "Fuzzy broad learning system: A novel neuro-fuzzy model for regression and classification," *IEEE Trans. Cybern.*, vol. 50, no. 2, pp. 414–424, Feb. 2018.

[34] M. Han, S. Feng, C. L. P. Chen, M. Xu, and T. Qiu, "Structured manifold broad learning system: A manifold perspective for large-scale chaotic time series analysis and prediction," *IEEE Trans. Knowl. Data Eng.*, vol. 31, no. 9, pp. 1809–1821, Sep. 2019.

[35] M. Xu, M. Han, C. L. P. Chen, and T. Qiu, "Recurrent broad learning systems for time series prediction," *IEEE Trans. Cybern.*, vol. 50, no. 4, pp. 1405–1417, Apr. 2020.

[36] S. Sui, C. L. P. Chen, S. Tong, and S. Feng, "Finite-time adaptive quantized control of stochastic nonlinear systems with input quantization: A broad learning system based identification method," *IEEE Trans. Ind. Electron.*, vol. 67, no. 10, pp. 8555–8565, Oct. 2020.

[37] J. Lin, Z. Liu, C. L. P. Chen, and Y. Zhang, "Quaternion broad learning system: A novel multi-dimensional filter for estimation and elimination tremor in teleoperation," *Neurocomputing*, vol. 380, pp. 78–86, Mar. 2020.

[38] F. Hasani and S. Shabanlou, "Weighted regularized extreme learning machine to model the discharge coefficient of side slots," *Flow Meas. Instrum.*, vol. 79, Jun. 2021, Art. no. 101955.

[39] M. Jiao, D. Wang, Y. Yang, and F. Liu, "More intelligent and robust estimation of battery state-of-charge with an improved regularized extreme learning machine," *Eng. Appl. Artif. Intell.*, vol. 104, Sep. 2021, Art. no. 104407.

[40] J. Qu, K. Ren, and X. Shi, "Binary grey wolf optimization-regularized extreme learning machine wrapper coupled with the Boruta algorithm for monthly streamflow forecasting," *Water Resour. Manage.*, vol. 35, no. 3, pp. 1029–1045, Feb. 2021.

[41] S. Sugimoto, R. Hamazaki, and M. Ueda, "Test of the eigenstate thermalization hypothesis based on local random matrix theory," *Phys. Rev. Lett.*, vol. 126, no. 12, Mar. 2021, Art. no. 120602.

[42] R. R. Li, M. D. Liebenthal, and A. E. DePrince, "Challenges for variational reduced-density-matrix theory with three-particle N-representability conditions," *J. Chem. Phys.*, vol. 155, no. 17, Nov. 2021, Art. no. 174110.

[43] S.-C. Yuan, J. Zhou, J.-X. Pan, and J.-Q. Shen, "Sphericity and identity test for high-dimensional covariance matrix using random matrix theory," *Acta Mathematicae Applicatae Sinica, English Ser.*, vol. 37, no. 2, pp. 214–231, Apr. 2021.

[44] M. Derezinski and M. W. Mahoney, "Determinantal point processes in randomized numerical linear algebra," *Notices Amer. Math. Soc.*, vol. 68, no. 1, pp. 34–45, 2021.

[45] A. Abdelfattah et al., "A survey of numerical linear algebra methods utilizing mixed-precision arithmetic," *Int. J. High Perform. Comput. Appl.*, vol. 35, no. 4, pp. 344–369, Jul. 2021.

[46] J. Zhao, Z. Wang, and D. S. Park, "Online sequential extreme learning machine with forgetting mechanism," *Neurocomputing*, vol. 87, pp. 79–89, Jun. 2012, doi: 10.1016/j.neucom.2012.02.003.

[47] H. Tian and P. Qin, "State of health prediction for lithium-ion batteries with a novel online sequential extreme learning machine method," *Int. J. Energy Res.*, vol. 45, no. 2, pp. 2383–2397, Feb. 2021.

[48] J. Ou, H. Li, G. Huang, and G. Yang, "Intelligent analysis of tool wear state using stacked denoising autoencoder with online sequential-extreme learning machine," *Measurement*, vol. 167, Jan. 2021, Art. no. 108153.

[49] C. Xiao, D. Sutanto, K. M. Muttaqi, M. Zhang, K. Meng, and Z. Y. Dong, "Online sequential extreme learning machine algorithm for better predispatch electricity price forecasting grids," *IEEE Trans. Ind. Appl.*, vol. 57, no. 2, pp. 1860–1871, Mar. 2021.
[50] Y. Guo, X. Yang, Y. Wang, F. Wang, and B. Chen, "Online robust echo state broad learning system," *Neurocomputing*, vol. 464, pp. 438–449, Nov. 2021.
[51] G. Feng, H. Wei, T. Qi, X. Pei, and H. Wang, "A transient electromagnetic signal denoising method based on an improved variational mode decomposition algorithm," *Measurement*, vol. 184, Nov. 2021, Art. no. 109815.
[52] W. Fu, P. Fang, K. Wang, Z. Li, D. Xiong, and K. Zhang, "Multi-step ahead short-term wind speed forecasting approach coupling variational mode decomposition, improved beetle antennae search algorithm-based synchronous optimization and Volterra series model," *Renew. Energy*, vol. 179, pp. 1122–1139, Dec. 2021.
[53] Y. Bai, M.-D. Liu, L. Ding, and Y.-J. Ma, "Double-layer staged training echo-state networks for wind speed prediction using variational mode decomposition," *Appl. Energy*, vol. 301, Nov. 2021, Art. no. 117461.
[54] Z. Zhang and W.-C. Hong, "Application of variational mode decomposition and chaotic grey wolf optimizer with support vector regression for forecasting electric loads," *Knowl.-Based Syst.*, vol. 228, Sep. 2021, Art. no. 107297.
[55] M. G. A. Nassef, T. M. Hussein, and O. Mokhiamar, "An adaptive variational mode decomposition based on sailfish optimization algorithm and Gini index for fault identification in rolling bearings," *Measurement*, vol. 173, Mar. 2021, Art. no. 108514.
[56] H. Hu, L. Wang, and R. Tao, "Wind speed forecasting based on variational mode decomposition and improved echo state network," *Renew. Energy*, vol. 164, pp. 729–751, Feb. 2021.
[57] L. Wang, H. Qiu, P. Yang, and L. Mu, "Arc fault detection algorithm based on variational mode decomposition and improved multi-scale fuzzy entropy," *Energies*, vol. 14, no. 14, p. 4137, Jul. 2021.
[58] M. Kumar, A. K. Bhandari, N. Singh, and A. Ghosh, "A new multilevel histogram thresholding approach using variational mode decomposition," *Multimedia Tools Appl.*, vol. 80, no. 7, pp. 11331–11363, Mar. 2021.
[59] J. Lian, Z. Liu, H. Wang, and X. Dong, "Adaptive variational mode decomposition method for signal processing based on mode characteristic," *Mech. Syst. Signal Process.*, vol. 107, pp. 53–77, Jul. 2018.
[60] Z. Wang, G. He, W. Du, J. Zhou, X. Han, J. Wang, H. He, X. Guo, J. Wang, and Y. Kou, "Application of parameter optimized variational mode decomposition method in fault diagnosis of gearbox," *IEEE Access*, vol. 7, pp. 44871–44882, 2019.
[61] A. Bagheri, O. E. Ozbulut, and D. K. Harris, "Structural system identification based on variational mode decomposition," *J. Sound Vib.*, vol. 417, pp. 182–197, Mar. 2018.
[62] F. Zhou, X. Yang, J. Shen, and W. Liu, "Fault diagnosis of hydraulic pumps using PSO-VMD and refined composite multiscale fluctuation dispersion entropy," *Shock Vib.*, vol. 2020, Aug. 2020, Art. no. 8840676, doi: 10.1155/2020/8840676.
[63] J. Liu, L. Luan, H. Wang, H. Peng, and H. Wang, "Fault detection of high voltage circuit breaker based on moving window variational mode decomposition and fuzzy entropy," in *Proc. IEEE Innov. Smart Grid Technol. Asia (ISGT Asia)*, May 2019, pp. 2005–2009, doi: 10.1109/ISGT-Asia.2019.8881417.

YANG LIU was born in Kaifeng, Henan, China, in 1979. She received the B.S. degree in computer application technology from Shanxi University, Taiyuan, in 2002, the M.S. degree in computer application technology from the University of Electronic Science and Technology of China, Chengdu, in 2005, and the Ph.D. degree in information and signal processing from the Institute of Optoelectronics Technology, Chinese Academy of Sciences, Chengdu, in 2012.

From 2002 to 2005, she studied at the University of Electronic Science and Technology of China. Since 2012, she has been working with the North China University of Water Resources and Electric Power. In 2015, she was an Associate Professor and a Postgraduate Tutor. She has presided over more than 20 scientific research projects. She has published more than 30 papers, including more than 20 papers included by SCI and EI. Her research interests include intelligent water conservancy, machine learning, and mathematical sequence analysis.

LIHU WANG received the B.S. degree in computer science from Xuchang University, in 2019. He is currently pursuing the M.S. degree in computer science with the North China University of Water Resources and Electric Power. His research interests include water conservancy big data, intelligent cloud computing, machine learning, and deep learning frontier knowledge and applications. His awards and honors include the North China University of Water Resources and Electric Power Scholarship and Internet Plus Innovation and Entrepreneurship Competition Contest Provincial Third Prize.

SHUAIBING DU was born in Pingdingshan, Henan, China, in 1995. He received the bachelor's degree from the Nanyang Institute of Technology, in 2019. He is currently pursuing the degree. He was admitted to the North China University of Water Resources and Hydropower, in 2020. His research interests include intelligent water conservancy, machine learning, and time series analysis.

LI ZHAO was born in Nanyang, Henan, China, in 1994. She received the B.S. degree in computer science and technology from the University of Jinan, in 2018. She is currently pursuing the master's degree with the North China University of Water Resources and Electric Power.

XUEMEI LIU received the M.S. degree from the Beijing University of Aeronautics and Astronautics, Beijing, China, in 1992, and the Ph.D. degree from Northwestern Polytechnical University, Xi'an, China, in 2008. Then, she spent several years as a Postdoctoral Researcher with the Beijing University of Aeronautics and Astronautics. She is currently a Professor and a Doctoral Supervisor with the North China University of Water Resources and Electric Power. Her current research interests include data mining, machine learning, virtual reality, and intelligent water conservancy.